Precision Engineering 40 (2015) 318–324

Contents lists available at ScienceDirect

Precision Engineering

journal homepage: www.elsevier.com/locate/precision

Technical note

Radial depth of cut stability lobe diagrams with process damping effects

Christopher T. Tyler, John Troutman, Tony L. Schmitz*

University of North Carolina at Charlotte, Mechanical Engineering and Engineering Science Department, 9201 University City Blvd., Charlotte, NC 28223, USA

ARTICLE INFO

Article history:
Received 31 January 2014
Received in revised form 17 October 2014
Accepted 9 November 2014
Available online 18 December 2014

Keywords:
Milling
Chatter
Process damping
Tool wear
CNC
CAM
Part path

ABSTRACT

This paper describes a method to produce analytical radial depth of cut stability lobe diagrams that include process damping. The stability limit was defined using the radial, rather than axial, depth due to the path planning approach for many computer-aided manufacturing (CAM) programs, which remove material layer-by-layer with a varying radial immersion. Experimental validation of the predicted stability limits was performed and the results are presented for both the process damping (low cutting speed) range and higher cutting speeds.

1. Introduction

Milling instability, or chatter, is one factor that limits material removal rates because the stable depth of cut is restricted by the system dynamics. Using the well-known stability lobe diagram, however, preferred (or "best") spindle speeds may be selected that enable the depth of cut to be increased [1–4]. These speeds occur at tooth passing frequencies that are integer fractions of the natural frequency that corresponds to the most flexible structural mode of vibration. Larger stable depths of cut are generally obtained at higher "best" spindle speeds.

A second primary limitation to high material removal rates is tool wear. Because diffusive tool wear is temperature-driven and higher cutting speeds lead to increased cutting temperatures, hard-to-machine materials may cause the higher "best" spindle speeds which provide access to increased depths of cut to be inaccessible due to unacceptable wear rates. Together, chatter and tool wear combine to increase machining costs and are, therefore, the subject of widespread modeling and experimental efforts.

One beneficial phenomenon that occurs at low spindle speeds (cutting speeds) and increases the allowable depth of cut is process damping. Many prior process damping studies have identified it as energy dissipation due to interference between the cutting tool clearance face and machined surface during relative vibrations between the two [5–24]. Because process damping enables increased material removal rates at low cutting speeds, it is an important consideration when modeling machining operations for hard-to-machine materials.

The purpose of machining models is to select optimal operating parameters at the process planning stage. For modern job shops, process planning begins with a solid model of the part to be machined. A computer-aided manufacturing (CAM) software package is then implemented to generate a computer-numerically controlled (CNC) part path from the solid model. For milling operations, the tool geometry, spindle speed, and feed per tooth must be specified in the CAM software. Additionally, the axial depth of cut and radial step-over must also be selected. Because material is often removed layer-by-layer, the axial depth of cut is fixed and the radial depth of cut is defined by the selected step-over. For internal pocketing operations, the radial depth varies with the tool location within the pocket for traditional path definitions, such as the spiral in strategy. In 90 deg corners, for example, the radial depth increases to an instantaneous value equal to the tool diameter regardless of the commanded step-over. For this reason, it is often desired to determine the limiting radial depth of cut as a function of spindle speed for a fixed axial depth; prior

* Corresponding author. Tel.: +1 17046875086.
E-mail address: tony.schmitz@uncc.edu (T.L. Schmitz).

http://dx.doi.org/10.1016/j.precisioneng.2014.11.004
0141-6359/

analytical efforts are described in [25,26]. However, traditional stability analyses assume a fixed radial depth and identify the maximum chatter-free axial depth for the selected range of spindle speeds.

The objective of this paper is to include the effects of process damping in a stability lobe diagram that describes the limiting radial depth of cut as a function of spindle speed. The work is particularly relevant for defining hard-to-machine material part programs. An analytical milling stability model that includes process damping [22–24] is applied to generate spindle speed versus axial depth stability limits for multiple radial depths. These limits are then combined automatically to identify the corresponding spindle speed versus radial depth stability lobe diagram for the selected axial depth. The paper is organized as follows. First, a review of the process damping model is provided. Second, the algorithm for identifying the required stability limit is described. Third, experimental results are provided. Finally, conclusions are presented.

2. Process damping

In descriptions of regenerative chatter in machining, the variable component of the instantaneous cutting force may be written as $F = K_s b(N_0 - N)$, where K_s is the specific cutting force, b is the chip width, N_0 is the vibration amplitude in the surface normal direction, n, from the previous cutting pass, and N is the current vibration amplitude. The underlying assumption in the force equation is that there is no phase shift between the variable force and chip thickness; this is indicated by the real values of K_s and b. However, for low cutting speeds, V, it has been shown that a phase shift can occur. This behavior is captured by the phenomenon referred to as process damping. Practically speaking, the effect of process damping is to enable significantly higher chip widths at low cutting speeds than linear stability analyses predict.

The process damping force in the n direction can be expressed as a function of velocity, chip width, cutting speed, and a constant C [21]: $F_d = -C\left(b/V\right)\dot{n}$. This process damping force was incorporated in Tlusty's stability algorithm in [22–24]. Tlusty's analytical stability solution assumes an average angle of the tooth in the cut, ϕ_{ave}, and, therefore, an average cutting force direction [3]. This assumption produces an autonomous, or time invariant, system. Tlusty then defined directional orientation factors, μ_x and μ_y, to first project the average angle force into the x and y mode directions and, second, project these results onto the surface normal (in the direction of ϕ_{ave}). The limiting axial depth of cut, b_{lim}, and spindle speed, Ω, expressions for milling are provided in Eqs. (1) and (2), where G_{or} is the oriented frequency response function that depends on the directional orientation factors and the frequency responses in the x and y directions, f_c is the chatter frequency, N is the number of complete vibration periods between teeth (i.e., the lobe number), N_t is the number of teeth on the cutter, and N_t^* is the average number of teeth in the cut; see Eq. (3), where ϕ_s and ϕ_e (deg) are the start and exit angles defined by the radial depth of cut. The fractional phase between the vibrations from one tooth to the next, ε, is defined in Eq. (4).

$$b_{\text{lim}} = \frac{-1}{2K_s Re\left[G_{\text{or}}\right] N_t^*} \tag{1}$$

$$\frac{f_c}{\Omega N_t} = N + \frac{\varepsilon}{2\pi} \tag{2}$$

$$N_t^* = \frac{\varphi_e - \varphi_s}{360/N_t} \tag{3}$$

$$\varepsilon = 2\pi - 2\tan^{-1}\left(\frac{Re\left(G_{\text{or}}\right)}{Im\left(G_{\text{or}}\right)}\right) \tag{4}$$

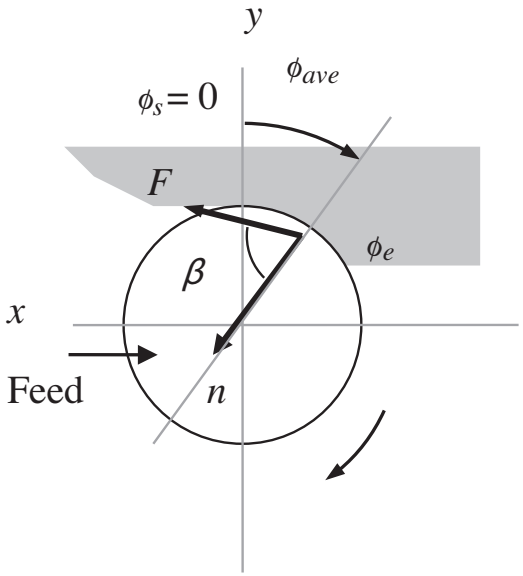

Fig. 1. Up milling geometry.

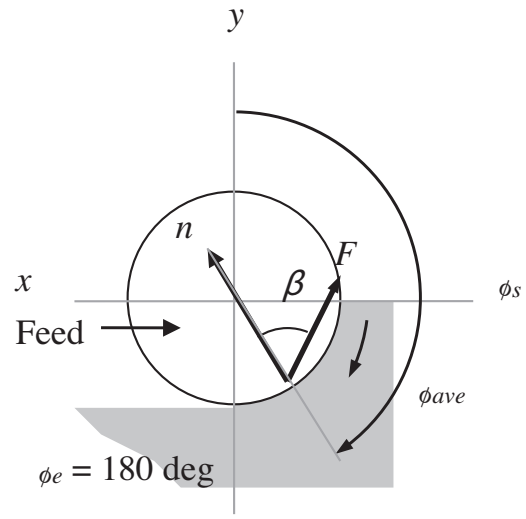

Fig. 2. Down milling geometry.

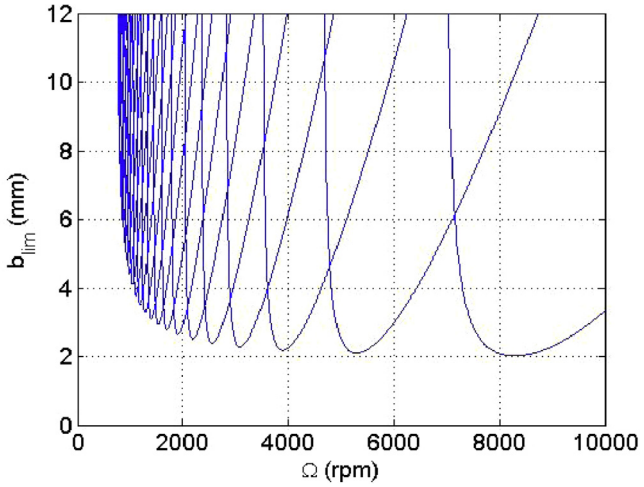

Fig. 3. Limiting axial depth of cut versus spindle speed for a 25% radial immersion.

The process damping force is incorporated by modifying the viscous (velocity-dependent) structural damping, c_x and c_y, in the x and y direction frequency response functions. For up (conventional) milling, the geometry is shown in Fig. 1, where n is the surface normal direction. The projection of the process damping force from the n direction onto the x direction is:

$$F_x = F_d \cos(90 - \phi_{ave}) = -C\frac{b}{V}\dot{n}\cos(90 - \phi_{ave})$$
$$= -\left(C\frac{b}{V}\cos(90 - \phi_{ave})\right)\dot{n}. \quad (5)$$

Substituting $\dot{n} = \cos(90 - \phi_{ave})\dot{x}$ in Eq. (5) gives:

$$F_x = -\left(C\frac{b}{V}\cos^2(90 - \phi_{ave})\right)\dot{x}. \quad (6)$$

The new viscous damping in the stability calculation for the x direction frequency response function, G_x, is therefore:

$$c_{new,x} = c_x + C\frac{b}{V}\cos^2(90 - \phi_{ave}). \quad (7)$$

The new y direction damping is:

$$c_{new,y} = c_y + C\frac{b}{V}\cos^2(180 - \phi_{ave}). \quad (8)$$

The oriented frequency response function is $G_{or} = \mu_x G_x + \mu_y G_y$, where $\mu_x = \cos\left(\beta - (90 - \phi_{ave})\right)\cos(90 - \phi_{ave})$ and $\mu_y = \cos\left(180 - \phi_{ave} - \beta\right)\cos(180 - \phi_{ave})$.

The geometry for the down (climb) milling case is shown in Fig. 2. Using the same approach as for up milling, the new x and y direction damping values are provided in Eqs. (9) and (10).

$$c_{new,x} = c_x + C\frac{b}{V}\cos^2(\phi_{ave} - 90) \quad (9)$$

$$c_{new,y} = c_y + C\frac{b}{V}\cos^2(180 - \phi_{ave}) \quad (10)$$

The oriented frequency response function for this case is $G_{or} = \mu_x G_x + \mu_y G_y$, where $\mu_x = \cos\left(\beta + \phi_{ave} - 90\right)\cos(\phi_{ave} - 90)$ and $\mu_y = \cos\left(\beta - (180 - \phi_{ave})\right)\cos(180 - \phi_{ave})$.

3. Radial depth stability limit

The spindle speed versus radial depth of cut stability lobe diagram is produced using the following sequence of steps.

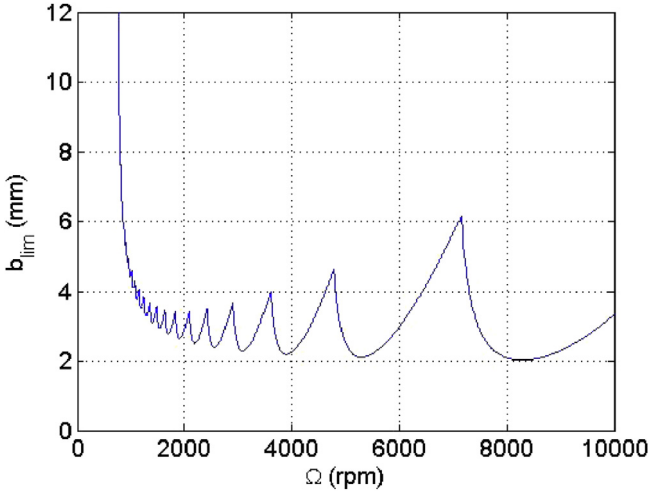

Fig. 4. Axial depth stability limit for a 25% radial immersion.

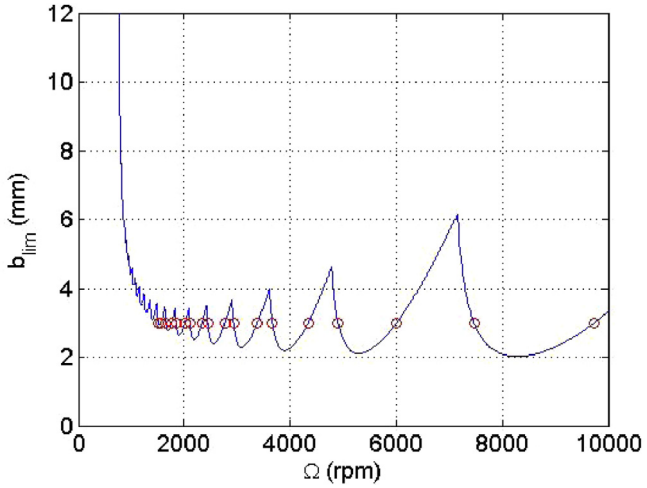

Fig. 5. Axial depth stability limit for a 25% radial immersion with the $b = 3$ mm spindle speeds identified (circles).

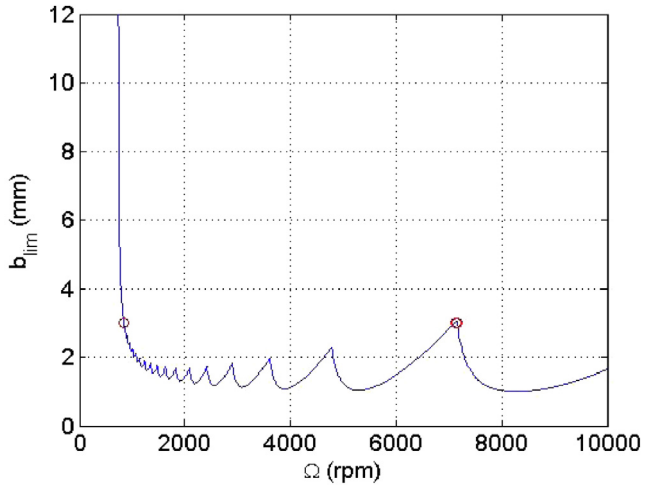

Fig. 6. Axial depth stability limit for a 50% radial immersion with the $b = 3$ mm spindle speeds identified (circles).

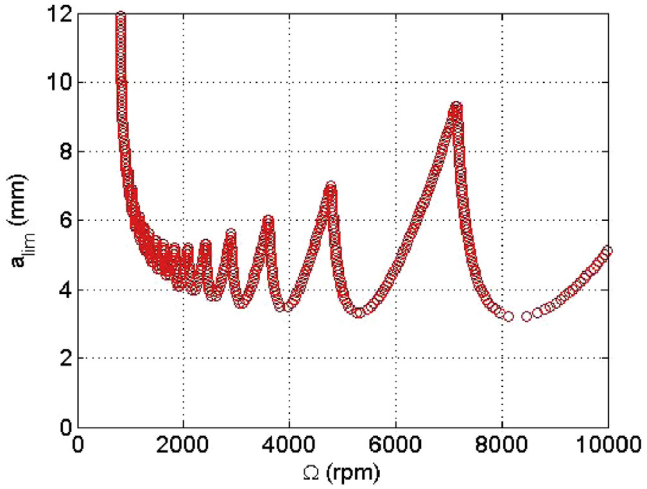

Fig. 7. Limiting radial depth of cut, a_{lim}, versus spindle speed for an axial depth of 3 mm.

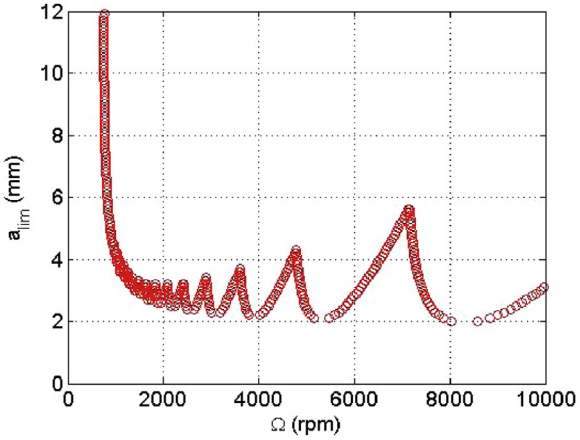

Fig. 8. Limiting radial depth of cut versus spindle speed for an axial depth of 5 mm.

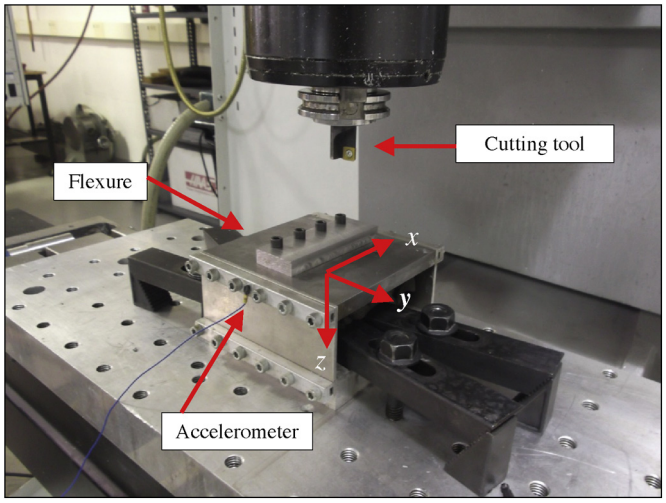

Fig. 9. Photograph of milling setup. The test coupon was bolted to the flexure. An accelerometer was used to measure the vibration during x direction cutting and identify stable and unstable conditions.

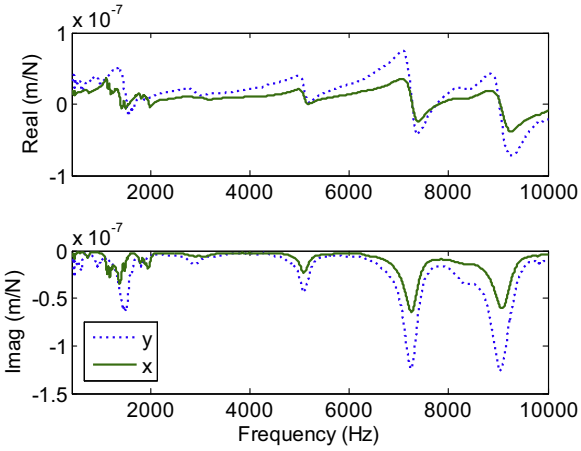

Fig. 10. Tool point frequency response functions in the x (solid line) and y (dotted line) directions.

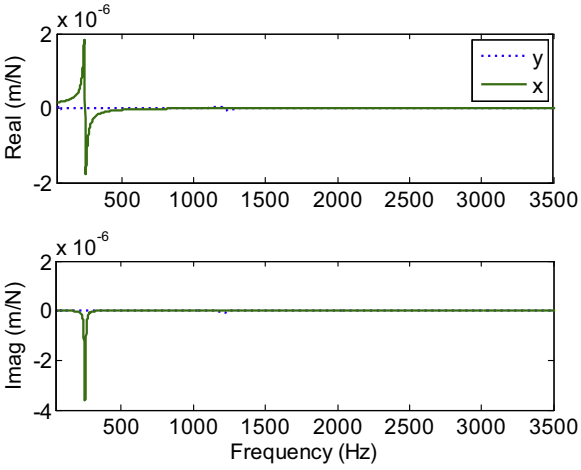

Fig. 11. Frequency response functions in the x (solid line) and y (dotted line) for the flexure.

(1) Specify the system dynamics, tool geometry, and force model, including both the cutting force and process damping coefficients.
(2) Select the desired spindle speed range and axial depth of cut.
(3) Generate the spindle speed versus axial depth stability lobe diagram for the selected dynamic system using the smallest desired radial depth of cut.
(4) Use the collection of stability lobes from step 3 to identify the limiting axial depth of cut as a function of spindle speed.
(5) Determine the spindle speeds at which the limiting axial depth is equal to the desired axial depth from step 2. Store these {spindle speed, radial depth} pairs.
(6) Increment the radial depth of cut to a larger value and repeat steps 3–5. Continue until the radial depth is increased to the tool diameter.
(7) Collect all {spindle speed, radial depth} pairs from steps 3–6. The result is the limiting radial depth of cut as a function of spindle speed. Because the axial depth of cut stability analysis

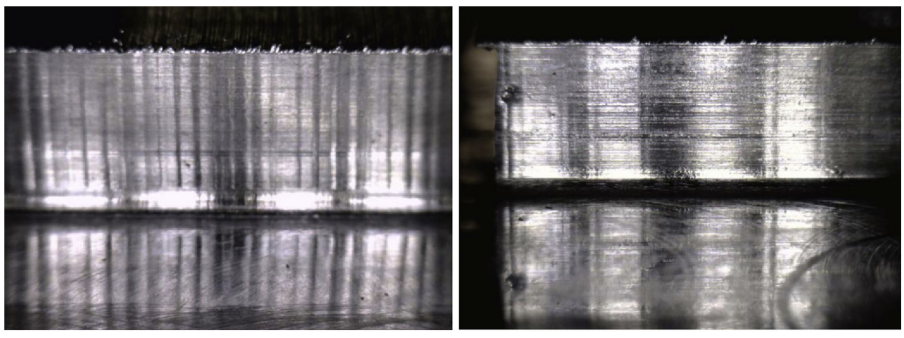

Fig. 12. Images of surfaces for unstable (left) and stable (right) cutting conditions.

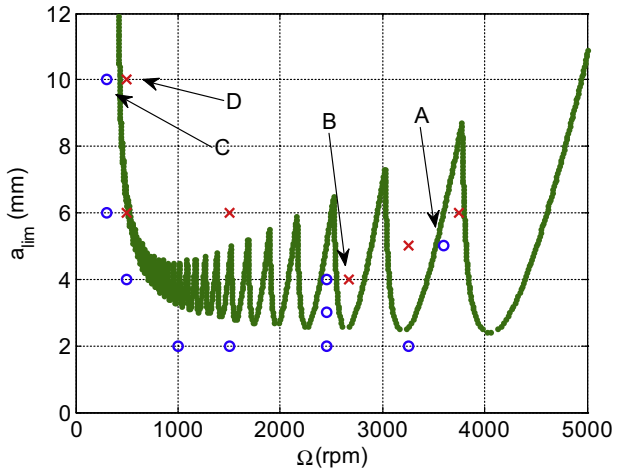

Fig. 13. Limiting radial depth of cut versus spindle speed for the flexure setup with a 3 mm axial depth.

includes process damping, the final radial depth stability limit also incorporates process damping effects.

The procedure steps are demonstrated through an example and the corresponding figures. For the example, the selected spindle speed range is zero to 10,000 rpm and the desired axial depth of cut is 3 mm. The spindle speed versus axial depth of cut stability lobe diagram for an up (conventional) milling radial depth of cut equal to 25% of the tool diameter (i.e., a 25% radial immersion) is displayed in Fig. 3. This represents the result from step 3. Fig. 4 shows the axial depth stability limit after step 4. The spindle speeds where the limiting axial depth is equal to the desired axial depth (b = 3 mm) for the final radial depth stability lobe diagram are identified in Fig. 5 (step 5). For comparison purposes, the step 5 result for a 50% radial immersion is shown in Fig. 6. It is observed that number of speeds is reduced with the increased radial depth because the axial depth stability limit is lowered. The final radial depth of cut stability lobe diagram (step 7) is displayed in Fig. 7. This represents the collection of limiting axial depths of cut identified over the full range of radial immersions (two examples for a desired axial depth of 3 mm are provided in Figs. 5 and 6). The corresponding diagram for a desired axial depth of 5 mm is provided in Fig. 8. As expected, the radial depth stability limit is lowered with the increased axial depth.

4. Experimental results

Milling experiments were performed to observe the effects of varying the radial depth of cut while maintaining a constant axial depth. A single tooth, 19.05 mm diameter, indexable end mill was used to machine AISI 1018 steel test coupons. The cutting inserts had a 0 deg rake angle and an 11 deg relief angle. The specific cutting force, K_s, and cutting force angle, β, were measured to be 2531.0 N/mm^2 and 62.0 deg, respectively, using a cutting force dynamometer (Kistler 9257B). A linear regression to the mean cutting force over a range of feed per tooth values was used to identify the force model values [27]. A process damping coefficient of

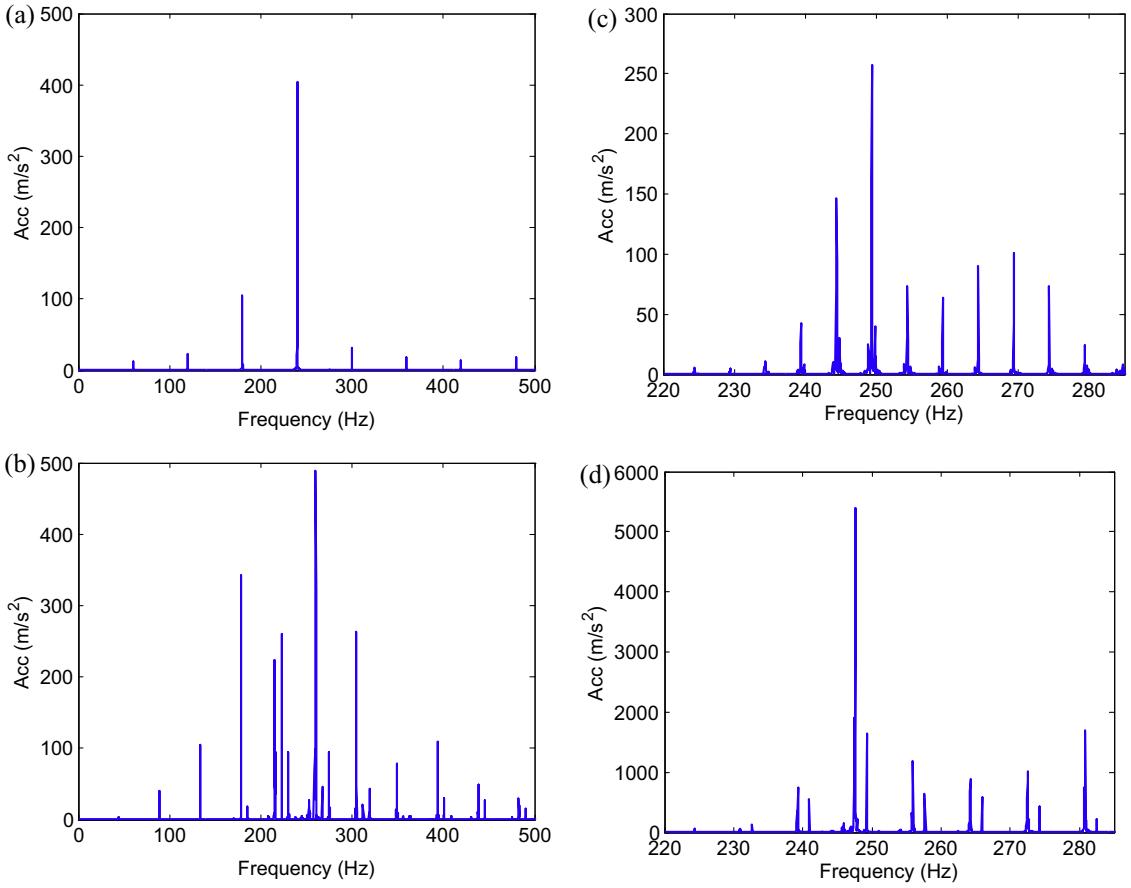

Fig. 14. (a) Frequency content for a stable cut at a spindle speed of 3600 rpm, a radial depth of 5 mm, and an axial depth of 3 mm. (b) Frequency content for an unstable cut at a spindle speed of 2675 rpm, a radial depth of 4 mm, and an axial depth of 3 mm. (c) Frequency content for a stable cut at a spindle speed of 300 rpm, a radial depth of 10 mm, and an axial depth of 3 mm. (d) Frequency content for an unstable cut at a spindle speed of 500 rpm, a radial depth of 10 mm, and an axial depth of 3 mm. Note the change in vertical scale relative to (a–c).

Table 1
Modal parameters for the flexure.

Direction	Modal stiffness (m/N)	Viscous damping ratio	Natural frequency (Hz)
x	6.60×10^6	0.021	247.2
y	338.0×10^6	0.015	1214

$C = 1.65 \times 10^5$ N/m was determined using the procedure described in [22–24].

A parallelogram, leaf-type flexure was constructed to provide a flexible base for the test coupons; see Fig. 9. The compliance of the platform in its flexible direction was approximately 14 times greater than that of the most flexible mode for the cutting tool–holder–spindle–machine assembly. The displacement-to-force frequency responses for the cutting tool and the flexure in the x (feed) and y directions are shown in Figs. 10 and 11. The modal parameters for the flexure are provided in Table 1.

The flexure's modal parameters, the tool geometry, and the cutting force model were used to generate radial depth of cut stability lobe diagrams for selected axial depths as described previously. To verify the stability predictions, cuts were completed at multiple {spindle speed, radial depth} pairs. A piezoelectric accelerometer (PCB Piezotronics model 352B10) was used to measure the flexure vibration during cutting. The frequency content of the accelerometer signal and the machined surface finish were used to characterize the stability. Cuts that exhibited significant frequency content near to the flexure's natural frequency, rather than at the tooth passing frequency and its harmonics were considered unstable. A comparison of surfaces from unstable and stable cuts is provided in Fig. 12; the images were obtained using a portable digital microscope.

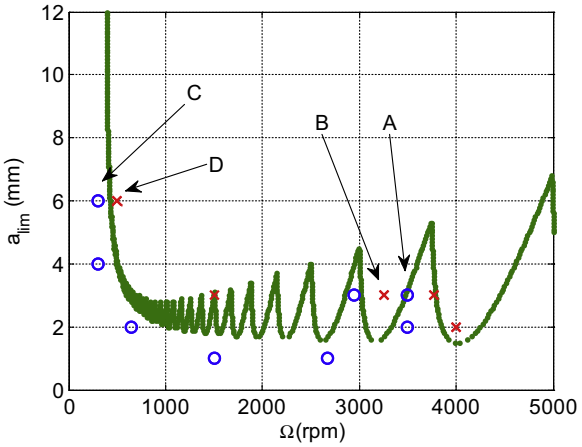

Fig. 15. Limiting radial depth of cut versus spindle speed for the flexure setup with a 5 mm axial depth.

Cutting tests were performed at two axial depths: 3 mm and 5 mm. In each case, a range of {spindle speed, radial depth} pairs were tested. Fig. 13 shows the predicted stability limit (•), as well as the stable (◯) and unstable cuts (×). Good agreement between the predicted limit and experimental results is observed for both the

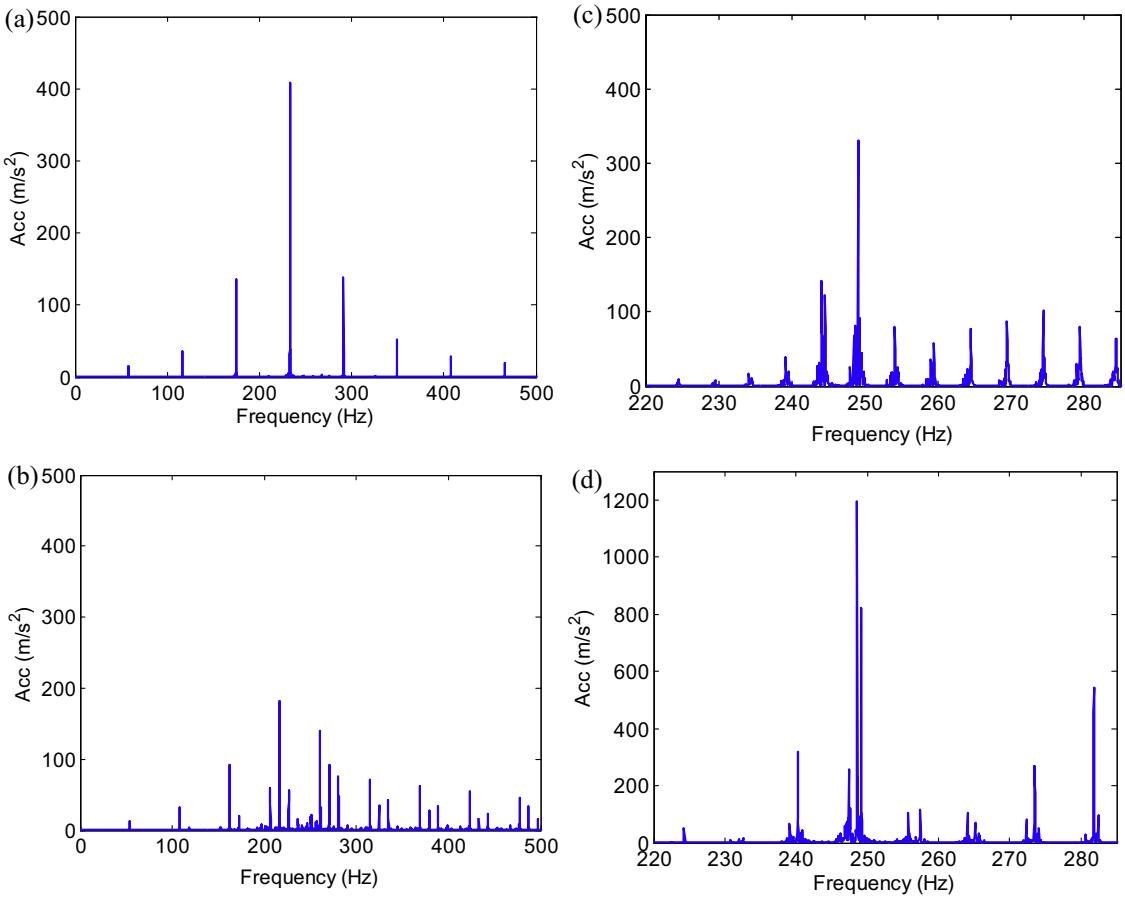

Fig. 16. (a) Frequency content for a stable cut at a spindle speed of 3500 rpm, a radial depth of 3 mm, and an axial depth of 5 mm. (b) Frequency content for an unstable cut at a spindle speed of 3250 rpm, a radial depth of 3 mm, and an axial depth of 3 mm. (c) Frequency content for a stable cut at a spindle speed of 300 rpm, a radial depth of 6 mm, and an axial depth of 5 mm. (d) Frequency content for an unstable cut at a spindle speed of 500 rpm, a radial depth of 6 mm, and an axial depth of 5 mm. Note the change in vertical scale relative to (a–c).

process damping regime (<1000 rpm) and higher cutting speeds. Fig. 14a–d shows the accelerometer frequency content at the test points labeled A through D in Fig. 13. Fig. 14b and d demonstrates unstable cutting conditions (points B and D in Fig. 13); significant content is seen near the flexure's natural frequency of 247.2 Hz in addition to the tooth passing frequency and its harmonics. Fig. 14a and c identify stable cuts with content at the tooth passing frequency and its harmonics only (points A and C).

Fig. 15 displays the predicted stability limit and experimental results for an axial depth of 5 mm. The increase in axial depth yields a decrease in the allowable radial depth relative to Fig. 13 (3 mm axial depth). Good agreement is again observed between the prediction and experimental results. Fig. 16a–d shows the frequency content for the points labeled A through D in Fig. 15. Points A and C (Fig. 16a and c) represent stable cuts, while points B and D (Fig. 16b and d) represent unstable cuts.

5. Conclusions

Radial depth of cut stability lobe diagrams were produced and verified experimentally. The motivation for describing the stability limit as radial, rather than axial, depth is the format for many CAM programs, which remove material layer-by-layer with a varying radial immersion. The analytical milling stability solution applied to identify the stability lobe diagrams included process damping, where the process damping model relied on a single coefficient, C. This is analogous to the specific cutting force, K_s, approach to modeling cutting force. Process damping is particularly important for hard-to-machine materials, such as titanium, nickel super alloys, and hardened steels. In these instances, tool wear generally prohibits higher surface speeds and the use of the large stable zones available at high spindle speeds.

Acknowledgement

The authors gratefully acknowledge partial financial support for this work from the UNC Charlotte Affiliates Program.

References

[1] Tlusty J, Polacek M. The stability of machine tools against self-excited vibrations in machining. In: Proceedings of the ASME international research in production engineering conference. 1963. p. 465–74 (3).
[2] Tobias SA. Machine tool vibrations. Glasgow: Blackie and Sons, Ltd; 1965.
[3] Tlusty J, Zaton W, Ismail F. Stability lobes in milling. Ann CIRP 1983;32/1:309–13.
[4] Altintas Y, Budak E. Analytical prediction of stability lobes in milling. Ann CIRP 1995;44/1:357–62.
[5] Wallace PW, Andrew C. Machining forces: some effects of tool vibration. J Mech Eng Sci 1965;7:152–62.
[6] Sisson TR, Kegg RL. An explanation of low-speed chatter effects. J Eng Ind 1969;91:951–8.
[7] Peters J, Vanherck P, Van Brussel H. The measurement of the dynamic cutting coefficient. Ann CIRP 1971;21/2:129–36.
[8] Tlusty J. Analysis of the state of research in cutting dynamics. Ann CIRP 1978;27/2:583–9.
[9] Wu DW. A new approach of formulating the transfer function for dynamic cutting processes. J Eng Ind 1989;111:37–47.
[10] Elbestawi MA, Ismail F, Du R, Ullagaddi BC. Modelling machining dynamics damping in the tool-workpiece interface. J Eng Ind 1994;116:435–9.
[11] Lee BY, Trang YS, Ma SC. Modeling of the process damping force in chatter vibration. Int J Mach Tools Manuf 1995;35:951–62.
[12] Abraria F, Elbestawi MA, Spencea AD. On the dynamics of ball end milling: modeling of cutting forces and stability analysis. Int J Mach Tools Manuf 1998;38:215–37.
[13] Ahmadi K, Ismail F. Machining chatter in flank milling. Int J Mach Tools Manuf 2010;50:75–85.
[14] Huang CY, Wang JJ. J Manuf Sci Eng 2007;129:12–20.
[15] Chiou YS, Chung ES, Liang SY. Analysis of tool wear effect on chatter stability in turning. Int J Mech Sci 1995;37:391–404.
[16] Chiou RY, Liang SY. Chatter stability of a slender cutting tool in turning with tool wear effect. Int J Mach Tools Manuf 1998;38:315–27.
[17] Chandiramani NK, Pothala T. Dynamics of 2-dof regenerative chatter during turning. J Sound Vib 2006;290:448–64.
[18] Jemielniak K, Widota A. Numerical simulation of non-linear chatter vibration in turning. Int J Mach Tools Manuf 1989;29:239–47.
[19] Ahmadi K, Ismail F. Experimental investigation of process damping nonlinearity in machining chatter. Int J Mach Tools Manuf 2010;50:1006–14.
[20] Budak E, Tunc LT. A new method for identification and modeling of process damping in machining. J Manuf Sci Eng 2009;131 (051019/1-10).
[21] Altintas Y, Eynian M, Onozuka H. Identification of dynamic cutting force coefficients and chatter stability with process damping. Ann CIRP 2008;57/1:371–4.
[22] Tyler C, Schmitz T. Process damping analytical stability analysis and validation. Trans NAMRI/SME 2012;40.
[23] Tyler C, Karandikar J, Schmitz T. Process damping coefficient identification using Bayesian inference. Trans NAMRI/SME 2013;41.
[24] C Tyler T, Schmitz T. Analytical process damping stability prediction. J Manuf Process 2013;15:69–76.
[25] Budak E, Tekeli A. Maximizing chatter free material removal rate in milling through optimal selection of axial and radial depth of cut pairs. CIRP Ann—Manuf Technol 2005;54/1:353–6.
[26] Zheng CM, Wang JJJ. Stability prediction in radial immersion for milling with symmetric structure. Int J Mach Tools Manuf 2013;75:72–81.
[27] Schmitz T, Smith S. Machining dynamics frequency response to improved productivity. New York, NY: Springer; 2009.